Chemo- and Magnetotaxis of Self-Propelled Light-Emitting Chemo-electronic Swimmers

Gerardo Salinas, Alice L. Dauphin, Camille Colin, Elena Villani, Stéphane Arbault, Laurent Bouffier, Alexander Kuhn

Chemo- and magnetotaxis of self-propelled light emitting chemo-electronic swimmers

Gerardo Salinas,[a] Alice L. Dauphin,[a] Camille Colin,[a] Elena Villani,[a] Stéphane Arbault,[a] Laurent Bouffier,[a] Alexander Kuhn*[a]

[a] Dr. G. Salinas, A. L. Dauphin, C. Colin, Dr. E. Villani, Dr. S. Arbault, Dr. L. Bouffier, Prof. A. Kuhn

Univ. Bordeaux, CNRS UMR 5255

Bordeaux INP, Site ENSCBP

F 33607 Pessac, France

E-mail: kuhn@enscbp.fr

Abstract: Miniaturized autonomous chemo-electronic swimmers, based on the coupling of spontaneous oxidation and reduction reactions at the two poles of light emitting diodes (LEDs), are presented as chemotactic and magnetotactic devices. In homogeneous aqueous media, random motion caused by a bubble-induced propulsion mechanism, is observed. However, in an inhomogeneous environment, the self-propelled devices exhibit positive chemotactic behavior, propelling themselves along a pH or ionic strength gradient (□pH, □I, respectively) in order to reach a thermodynamically higher active state. In addition, the intrinsic permanent magnetic moment of the LED allows self-orientation in the terrestrial magnetic field or following other external magnetic perturbations, which enables a directional motion control coupled with light emission. The interplay between chemotaxis and magnetotaxis allows fine-tuning the dynamic behavior of these swimmers.

Introduction

Self-propulsion of swimmers that transform different types of energy into mechanical motion, has gained considerable interest in recent years.[1-4] These devices enable interesting applications in drug delivery,[5] cargo-lifting,[6] sensing,[7] environmental remediation,[8] lab-on-a-chip devices (e.g. pumps or mixers)[9] and as models to mimic and understand collective behavior of microorganisms.[10-13] Recently, a significant number of nano, micro and macro-swimmers powered by the decomposition of “fuels” (e.g. H2O2),[14-15] external electric or magnetic fields,[16-19] surface tension gradients (Marangoni effect),[20-23] self-diffusiophoresis or electrophoresis,[24-25] has been described. Since at small scales (from □m to nm) Brownian collisions or surface phenomena become dominant, the design, synthesis and motion control of self-propelled swimmers still remain the main challenges in this field. An interesting approach is the possible use of microelectronics (e.g. semiconductor diodes) as self-propelling electronic swimmers (e-swimmers). These devices provide the unique feature of coupling motion with an electronic response such as light emission.[26-28] Velev et al. demonstrated motion control of semiconductor diodes at the air/water interface by an electroosmotic mechanism in the presence of an external electric field.[26] Furthermore, the electric field does not only provide directional control, but also allows to switch on and off the electronic response of these e-swimmers. Although directional control is desired, autonomous motion is the key to understand collective behavior. A promising alternative is the design of autonomous e-swimmers powered by spontaneous chemical reactions connected to the electrical terminals of the microelectronics. If the involved redox reactions are well-chosen, a sufficient potential difference can be generated to overcome the threshold voltage necessary to switch on these devices. In this work, we introduce such a chemo-electronic swimmer, based on the coupling of the oxidation of Mg and

the reduction of H3O+. Furthermore, the ferromagnetic components of the swimmers enable magnetotactic behavior as a promising alternative to chemotaxis.

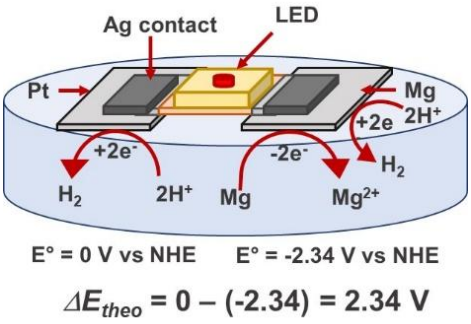

Scheme 1. Principle of a modified light emitting diode swimming at an air/water interface and powered by the spontaneous oxidation of a Mg foil and the reduction of H3O+ on the Pt and Mg foils.

Results and Discussion

Chemo-electronic swimmers

The swimmers were built by attaching small pieces of Mg and Pt foils to the anode and cathode, respectively, of a miniature red light-emitting diode (LED) (Scheme 1). Theoretically, in acidic solution, oxidation of Mg and reduction of H3O+ on Pt occur spontaneously with a standard redox potential difference of 2.34 V (Etheo). Experimentally, a redox potential difference (Eexp) of 1.57 0.01 V was measured at the air/water interface of a 20 mM H2SO4/0.125 mM sodium dodecyl sulfate (SDS) solution, which is slightly above the threshold potential of the used LED (1.55 V, Figure S1), thus allowing to switch on the device.

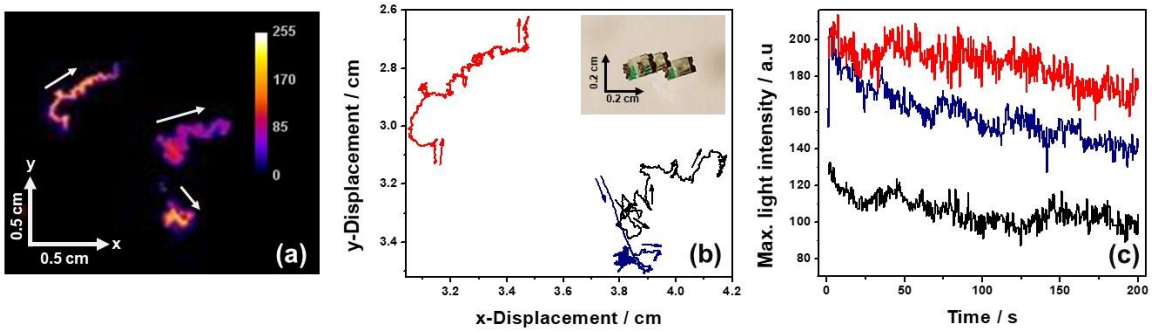

Figure 1. (a) Tracking of the maximum light intensity of three independent chemo-electronic swimmers moving on the air/water interface of a 20 mM H2SO4/0.125 mM SDS solution. (b) Trajectory plot and (c) time evolution of the light intensity for the three chemo-electronic swimmers. The inset in (b) shows as a control experiment the accumulated day light images of an unmodified LED at t0 and after 5 minutes in order to demonstrate the absence of motion.

The autonomous motion of a modified diode, carefully positioned (Scheme S1) at the air/water interface of a 20 mM H2SO4/0.125 mM SDS solution, was monitored by video-macroscopy recordings of its light emission. In a homogeneous acidic solution, these chemo-electronic swimmers show stepwise motion at the 2-dimensional interface (random walk) with an average speed of 0.175 ± 0.075 mm s-1 ($\bar{v}$_(H_2 〖SO〗 _4)) (Figure 1a and 1b, Video S1), accompanied by a slowly decreasing light emission (Figure 1a and 1c). The latter is attributed to the adhesion of H2 bubbles, which gradually block the access of H3O+ to the surface of the metal plates. Under these conditions, the involved redox reactions are powering two different processes; (i) the light emission of the diode, and (ii) the mechanical propulsion via the generated hydrogen bubbles. The amplitude of both processes is intimately related to the corrosion rate of the magnesium. However, the light intensity will also depend on the fraction of hydrogen not directly formed at the Mg surface, but rather at the Pt surface, since this requires the shuttling of the electrons through the LED. Recording the bottom view of the swimmer/H2O interface during the reaction provides more information about the main site of bubble formation (Figure S2). Although LED emission confirms the reduction of H3O+ on the Pt surface, a more pronounced H2 bubble formation is observed at the Mg surface. From a thermodynamic point of view, H2 bubble formation occurs on both metallic plates since the global redox reaction (equation 1) takes place spontaneously (ΔG°(1) = –451.6 kJ mol-1). Nevertheless, on the Mg surface an additional reaction further promotes the pronounced H2 bubble formation. In aqueous media, the reaction between water and Mg, which generates Mg(OH)2 and H2 bubbles, is thermodynamically favorable (ΔG°(2) = –1125.6 kJ mol-1) (Equation 2).

Mg+ 〖2H〗 ^+→ 〖Mg〗 ^(2+)+H_2 (1)

Mg+ 〖2H〗 _2 O↔ 〖Mg(OH)〗 _2+H_2 (2)

Furthermore, the presence of a strong acid improves dissolution of the Mg(OH)2 layer by means of an acid-base reaction, enabling the access of H3O+ to the Mg surface and eventually improving the H2 bubble formation. We therefore can conclude that the dominant driving force for the motion in the form of bubble generation is located at the Mg side of the LED.

Chemotaxis

In order to test the possible chemotactic behavior of the swimmers, motion of these devices in the presence of two different concentration gradients, [H2SO4] and [MgSO4] (ΔpH and Δ[MgSO4]), was evaluated. Chemotaxis is a well-known biological phenomenon, exemplified by motion of microorganisms towards food sources (positive chemotaxis) or away from toxins (negative chemotaxis).[29] Chemotactic behavior of self-propelled swimmers, sensitive to different chemical gradients (e.g. H2O2, pH and surfactants) has already been reported.[1],[13],[30] Commonly, chemotaxis occurs when a self-propelled swimmer has at least one active site which is sensitive to a chemical signal.[30] Since our modified diode presents two active sites which can react with H3O+, chemotactic behavior was anticipated and studied in detail.

The motion of the chemo-electronic swimmer was probed on the air/water interface of a 0.125 mM SDS aqueous solution where a ΔpH is established. Swimmers show a positive chemotactic effect (Figure 2a and Video S2) since they move towards locations with a higher proton concentration. Initially (t ≈ 20 s), the speed and the intensity of emitted light are roughly constant and low, due to a low [H3O+] concentration ($\bar{v}$_(t<20s) = 0.18 ± 0.04 mm s-1) (Figure 2b and Figure S3a). Subsequently, speed increases, first with a moderate acceleration (zone a1 = 0.02 mm s-2) when the swimmer senses a weak gradient, followed by a more pronounced acceleration (zone a2 = 0.49 mm s-2) when it enters the zone of high ΔpH. Concomitantly, the LED light intensity increases (Figure 2b). These

successive acceleration steps are in agreement with the pH values observed in Figures S3b-c, since the speed increases as the chemo-electronic swimmer enters regions where ∇pH is steeper. This is a clear evidence that the increase in [H3O+] at the metallic surfaces leads to a faster bubble formation and thus to an improvement of the propulsion. Although, bubble propulsion based on H3O+ consumption is a reasonable explanation for the motion of the swimmer in acidic media, other parameters might also affect its dynamic behavior. As one of the reactions involves oxidative dissolution of Mg, one might expect, based on the Nernst equation, that the [Mg2+] concentration in solution should also influence the driving force. From a thermodynamic point of view, the swimmer should move away from ∇[MgSO4] as Mg2+ is expected to act as a chemo-repellent (i.e. negative chemotaxis). However, unexpectedly the device placed at the air/water interface of a homogeneous 5 mM H2SO4 solution directs itself towards ∇[MgSO4] (Figure 2c and Video S3) with a rather constant speed ($\bar{v}$_(Mg〖SO〗_4) = 0.21 ∇ 0.09 mm s-1) and a decrease of light intensity (Figure 2d).

In order to better understand the origin of this behavior, similar experiments with gradients of another cation were carried out. The motion on the air/water interface of a homogeneous 5 mM H2SO4 aqueous solution, in the presence of a [Na2SO4] gradient (∇[Na2SO4]), shows also a positive chemotactic effect (Figure S4a, b). Similar average speed ($\bar{v}$_(〖Na〗_2 〖SO〗_4) = 0.26 ∇ 0.05 mm s-1) and light intensity profiles were obtained. In order to elucidate the respective roles of protons and the additional cation, experiments were performed in the absence of sulfuric acid. In the absence of a good proton donor, the spontaneous formation of a Mg(OH)2 layer on the surface of the anode should limit the redox reactions, and hence the H2 bubble formation. Nonetheless, in the presence of both cation gradients, the motion of the swimmer reveals a positive chemotactic effect (Figure S5) with a comparable average speed ($\bar{v}$_(Mg〖SO〗_4) = 0.18 mm s-1, and $\bar{v}$_(〖Na〗_2 〖SO〗_4) = 0.22 mm s-1). These results indicate that the motion must be related to the sensitivity of Mg corrosion not only to proton concentration, but should also depend on the total ionic strength I and the nature of the anion. Improvement of corrosion by dissolution of the Mg(OH)2 layer in solutions with a higher I has been previously observed for spherical Mg/Pt, Mg/Au and Mg/Pt-Poly(N-isopropylacrylamide) Janus particles. [31-34] As stated above, in aqueous media, water reacts spontaneously with Mg to generate Mg(OH)2 and H2 bubbles (equation 2), and such a layer can be dissolved in the presence of sulfate anions, following equation (3), analogue to what has been reported.[31]

〖Mg(OH)〗_2+〖SO〗_4^(2-)↔〖MgSO〗_4+〖2OH〗^- (3)

When the sulfate concentration is sufficiently high, equilibria shift towards the product formation, dissolving the Mg(OH)2 layer, enabling the access of water to the Mg surface and eventually improving the H2 bubble formation. Therefore, the chemo-electronic swimmer moves towards the ∇I in order to reach a thermodynamically higher active state. From the calculated I values of the initial 2 M solution of sulfate salt (I = 8 M and I = 6 M for MgSO4 and Na2SO4, respectively)[35] it can be deduced that the chemo-electronic swimmers move towards positions where ∇I is steeper. A control experiment evaluating the motion in the presence of a [NaCl] gradient showed as well a positive chemotactic effect with a significant increase of the average speed, in comparison with the corresponding sulfate salt ($\bar{v}$_NaCl = 0.52 mm s-1) (Figure S5c). This is in agreement with the different values of corrosion rate reported for magnesium alloys, revealing that the corrosion process is favored in the presence of chloride anions.[32-34],[36] Furthermore, a bottom-view of the swimmer/H2O interface showed for homogeneous electrolyte solutions of MgSO4 or Na2SO4, a predominant bubble formation on the Mg anode (Figure S6). Therefore, motion in electrolyte gradients is as well based on a bubble propulsion mechanism triggered by Mg corrosion. This control experiment illustrates that, although the diode switches on simultaneously with the corrosion

process, light intensity fades-out since hydrogen evolution is preferentially occurring at the Mg site and consequently less electrons will be delivered to the Pt site across the LED. Finally, from Figure S5 it can be seen that at the beginning of the motion, the chemo-electronic swimmers automatically align themselves with respect to the chemical gradient. When the symmetry axis of the swimmer is misaligned with the chemical gradient, the spatial distribution of hydrogen production is anisotropic. Therefore, the swimmer rotates until its symmetry axis is aligned with the direction of the chemical gradient.[37]

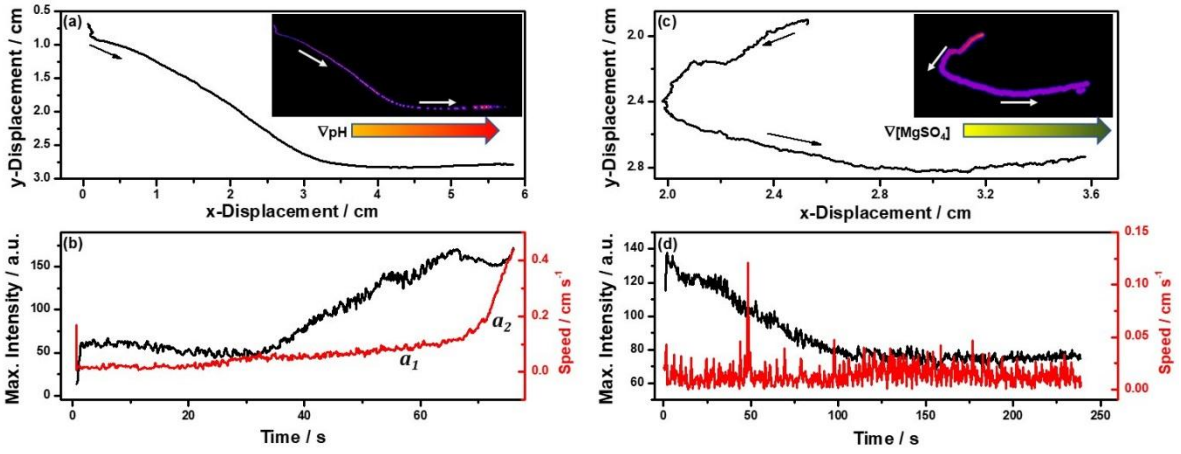

Figure 2. (a) Trajectory of a single swimmer moving on the air/water interface of a 0.125 mM SDS solution in the presence of a generated ∇pH and (b) time-evolution of the light intensity (left axis) and speed profile (right axis) versus time. (c) Trajectory of a swimmer moving on the air/water interface of a 5 mM H2SO4 solution in the presence of a ∇[MgSO4] and (d) time-evolution of the light intensity (left axis) and speed profile (right axis) versus time. Insets show the tracking of the maximum light intensity for videos S2 and S3.

Magnetotaxis

Another interesting feature of these microelectronic devices is their intrinsic magnetic properties, due to the presence of ferromagnetic metals in the LED components.[38-39] At the air/water interface, the diodes self-orientate surprisingly well and in a robust way with respect to the terrestrial magnetic field (Figure S7a). Furthermore, by approaching the south pole of a magnet (1.18 Tesla), the diode self-aligns with respect to the imposed external magnetic field (Figure S7b-c), whereas after removal of the perturbation the diode returns back to its initial position imposed by the terrestrial field (Figure S7d-e). It has to be pointed out that the direction of the small permanent magnetic moment of the diodes is not always parallel to the main axis of the diode. Its direction can be modified by magnetization with a strong permanent magnet. These results are clear evidence of the presence of an intrinsic magnetic moment in the sole diode, which allows studying the magnetotactic behavior of the designed swimmers. Magnetotaxis is the phenomenon where a particle with a permanent magnetic moment orientates itself towards the magnetic field of the earth or with respect to an external magnetic field.[40] This was first observed for iron-rich magnetotactic microorganisms,[41-42] and then the same concept was used to develop magnetotactic micro and nano-swimmers.[43-46] Magnetotaxis offers a supplementary level of control through directional

motion in a wireless non-invasive way.[44],[47-49] This phenomenon should not be confused with propulsion powered by alternating magnetic fields, where rotational or undulatory motion is transformed into translational motion.[17], [19], [50-51]

At a first stage, when placed at the air/water interface the swimmers align with respect to the magnetic field of the earth and can be reoriented with an imposed magnetic field (Figure S8a). A similar behavior was observed at the air/water interface of different homogeneous solutions of H2SO4 and MgSO4, meaning that prior to the observed characteristic random motion the initial orientation remains unaffected (Figure S8b, c). Since the magnetotactic effect in a homogeneous acidic solution provides the unique opportunity of coupling guided motion with an electronic response leading to light emission, the magnetotaxis of the swimmers was evaluated. Motion of the chemo-electronic swimmer at the air/water interface of a homogeneous 10 mM H2SO4 solution, in the presence of an external magnetic field gradient (∇B⃗), revealed an initial phase of alignment with the magnetic field, followed by a linear motion towards the north pole of the magnet (Figure 3a and Video S4). During the first period (t ≈ 15 s), the speed of the swimmer increases slowly (Figure 3b) due to a low ∇B⃗, accompanied by a slight decrease of the light intensity caused by the adhesion of H2 bubbles to the surface of the metal plates. Subsequently, as the distance from the magnet decreases and ∇B⃗ increases, an exponential increase of the speed was observed, reaching a maximum value of 10.79 cm s-1 until the swimmer hits the magnet. At such high-speed the Mg surface is not blocked due to a hydrodynamic bubble removal, which promotes the proton reduction on the Mg surface, more favorably than on the Pt surface, thus causing a considerable decrease of light intensity. These first results prove the magnetotactic behavior of the designed chemo-electronic swimmers, which may be used for directional control coupled with light emission.

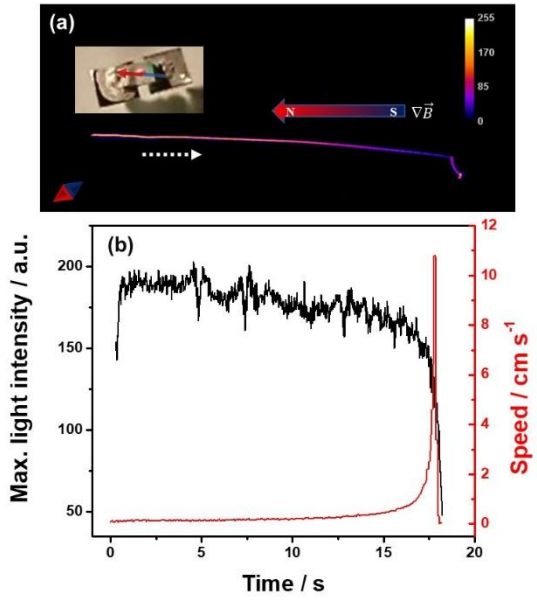

Figure 3. (a) Tracking of the maximum light intensity of video S4 that shows the trajectory together with the light intensity of a swimmer moving at the air/water interface of a homogeneous 10 mM H2SO4 solution in the presence of a ∇B⃗ (b) light intensity (left axis) and speed profile (right axis) versus time. Inset: daylight image of the swimmer orientation at the beginning of the experiment.

Coupled chemo- and magnetotactic motions

Due to the presence of both chemo- and magnetotactic features in the chemo-electronic swimmer, a possible synergy between both mechanisms was evaluated. Two different ∇pH gradients established

by addition of 1 mL of a 50 mM or 10 mM H2SO4 solution were used (□pH1 and □pH2, respectively). Before the generation of the □pH, the modified LED self-aligns with respect to the terrestrial magnetic field, as discussed above (Figure 4a). Then the chemo-electronic swimmer is deliberately placed in a position where its intrinsic magnetic moment is not aligned with the terrestrial magnetic field but has the right orientation with respect to the chemical gradient (Figure 4b). In the presence of □pH1, chemotaxis is able to partially overcome the terrestrial magnetic field, since the swimmer keeps its initial orientation and moves towards the chemical gradient (Video S5). However, its overall trajectory (T1 in Figure 4) is not directly following the chemical gradient. A competition between the vector of the chemical gradient and the vector of the terrestrial magnetic field provides a suitable explanation for this trajectory. As it can be seen from Figure 4c, at the end of the motion, the symmetry axis of the swimmer is aligned with the new trajectory. Therefore, T1 is the result of the vector addition between the chemical gradient and the terrestrial magnetic field (Figure 4d). Finally, in the presence of □pH2 (smaller compared to □pH1) a new trajectory (T2 in Figure 4) is observed. For this □pH the vector of the terrestrial magnetic field becomes dominant with respect to the vector of the chemical gradient and the trajectory correlates with the vector addition shown in Figure 4e. Such a synergy between both gradients also explains the trajectory observed in Figure 2a. At t □ 20 s the terrestrial magnetic field dominates the chemical gradient and the swimmer moves almost orthogonal to the □pH vector. As the swimmer moves into a steeper □pH (20 □ t □ 70 s), the chemical gradient starts to compete more strongly with the terrestrial magnetic field and the direction of the trajectory is the vector addition of both forces. Finally, at t > 70 s the chemical gradient completely dominates the terrestrial magnetic field and the swimmers moves parallel to the □pH vector.

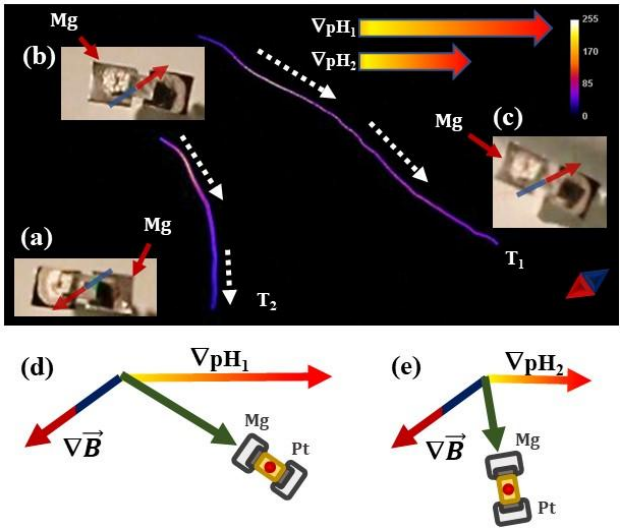

Figure 4. Tracking of the maximum light intensity of two-independent chemo-electronic swimmers moving at the air/water interface in the presence of two different □pH. Image of a chemo-electronic swimmer in (a) the absence of a □pH, (b) initial and (c) final orientation in the presence of □pH1. Schematic illustration of the vector addition of (d) trajectory 1 (T1) and (e) trajectory 2 (T2). The translucent arrows indicate the magnetic moment of the diode.

Conclusion

In conclusion, we present the first example of a chemo-electronic swimmer, combining a bubble propulsion mechanism with light emission triggered by Mg corrosion. The self-propelled devices show positive chemotactic behavior, propelling themselves towards a chemical gradient (□pH or □I) in order to reach a thermodynamically higher active state. Finally, the presence of a small internal permanent magnetic moment allows the swimmers to sense the terrestrial magnetic field or to

orient with respect to an external magnetic perturbation, thus enabling directional control, coupled with light emission. Last but not least, the interplay between chemotactic and magnetotactic forces gives a unique possibility to generate and control more complex trajectories.

Acknowledgements

The project has been funded by the European Research Council (ERC) under the European Union's Horizon 2020 research and innovation program (grant agreement no 741251, ERC Advanced grant ELECTRA). ALD acknowledges the University of Bordeaux for her PhD scholarship.

Keywords: Chemotaxis • electronic swimmers • pH gradient • light emission • magnetotaxis

[1] W. Wang, W. Duan, S. Ahmed, T. E. Mallouk, A. Sen, Nano Today 2013, 8, 531-554.

[2] C. W. Shieds IV, O. D. Velev, Chem. 2017, 3, 539-559.

[3] S. Sanchez, L. Soler, J. Katuri, Angew. Chem. Int. Ed. 2015, 54, 1414-1444.

[4] J. Wang, Nanomachines: Fundamentals and Applications, Wiley, 2013.

[5] D. Kagan, R. Laocharoensuk, M. Zimmerman, C. Clawson, S. Balasubramanian, D. Kang, D. Bishop, S. Sattayasamitsathit, L. Zhang, J. Wang, Small 2010, 6, 2741-2747.

[6] G. Loget, A. Kuhn, Lab Chip 2012, 12, 1967-1971.

[7] M. Zarei, M. Zarei, Small 2018, 14, 1800912.

[8] W. Gao, J. Wang, ACS Nano 2014, 8, 3170-3180.

[9] S. T. Chang, E. Beaumont, D. N. Petsev, O. D. Velev, Lab Chip 2008, 8, 117-124.

[10] C. Chen, X. Chang, H. Teymourian, D. E. Ramirez-Herrera, B. Esteban-Férnandez de Ávila, X. Lu, J. Li, S. He, C. Fang, Y. Liang, F. Mou, J. Guan, J. Wang, Angew. Chem. Int. Ed. 2018, 57, 241-245.

[11] Q. He, Y. Ji, X. Lin, Z. Wu, Y. Wu, W. Gao, Angew. Chem. Int. Ed. 2019, 58, 12200-12205.

[12] L. Baraban, S. M. Harazim, S. Sánchez, O. G. Schmidt, Angew. Chem. Int. Ed. 2013, 52, 5552-5556.

[13] J. Plutnar. M. Pumera, Angew. Chem. Int. Ed. 2019, 58, 2190-2196.

[14] Y. Wang, R. M. Hernandez, D. J. Bartlett, J. M. Bingham, T. R. Kline, A. Sen, T. E. Mallouk, Langmuir 2006, 22, 10451-10456.

[15] Z. Fattah, G. Loget, V. Lapeyre, P. Garrigue, C. Warakulwit, J. Limtrakul, L. Bouffier, A. Kuhn, Electrochim. Acta 2011, 56, 10562-10566.

[16] L. Bouffier, V. Ravaine, N. Sojic, A. Kuhn, Curr. Opin. Colloid Interface Sci. 2016, 21 57-64.

[17] K. Han, C. W. Shields IV, O. D. Velev, Adv. Funct. Mater. 2018, 28, 1705953.

[18] W. Gao, K. M. Manesh, J. Hua, S. Sattayasamitsathit, J. Wang, Small 2011, 7, 2047-2051.

[19] T. Li, J. Li, H. Zhang, X. Chang, W. Song, Y. Hu, G. Shao, E. Sandraz, G. Zhang, L. Li, J. Wang, Small 2016, 12, 6098-6105.

[20] R. Sharma, S. T. Chang, O. D. Velev, Langmuir 2012, 28, 10128-10135.

[21] T. H. Seah, G. Zhao, M. Pumera, ChemPlusChem 2013, 78, 395-397.

[22] G. Zhao, T. H. Seah, M. Pumera, Chem. Eur. J. 2011, 17, 12020-12026.

[23] G. Zhao, M. Pumera, Lab Chip 2014, 14, 2818-2823.

[24] W. F. Paxton, S. Sundarajan, T. E. Mallouk, A. Sen, Angew. Chem. Int. Ed. 2006, 45, 5420-5429.

[25] S. Sengupta, M. E. Ibele, A. Sen, Angew. Chem. Int. Ed. 2012, 51, 8434-8445.

[26] S. T. Chang, V. N. Paunov, D. N. Petsev, O. D. Velev, Nat. Mater. 2007, 6, 235-240.

[27] R. Sharma, O. D. Velev, Adv. Funct. Mater. 2015, 25, 5512-5519.

[28] J. Roche, S. Carrara, J. Sanchez, J. Lannelongue, G. Loget, L. Bouffier, P. Fischer, A. Kuhn, Sci. Rep. 2014, 4, 6705.

[29] B. Liebchen, H. Löwen, Acc. Chem. Res. 2018, 51, 2982-2990.

[30] M. N. Popescu, W. E. Uspal, C. Bechinger, P. Fischer, Nano Lett. 2018, 18, 5345-5349.

[31] F. Mou, C. Chen, H. Ma, Y. Yin, Q. Wu, J. Guan, Angew. Chem. Int. Ed. 2013, 52, 7208-7212.

[32] W. Gao, X. Feng, A. Pei, Y. Gu, J. Li, J. Wang, Nanoscale 2013, 5, 4696-4700.

[33] D. Rojas, B. Jurado-Sánchez, A. Escarpa, Anal. Chem. 2016, 88, 4153-4160.

[34] F. Mou, C. Chen, Q. Zhong, Y. Yin, H. Ma, J. Guan, ACS Appl. Mater. Interfaces 2014, 6, 9897-9903.

[35] J. D. Willey, J. Chem. Educ. 2004, 81, 1644-1646.

[36] L. Wang, T. Shinohara, B. P. Zhang, J. Alloys Compd. 2010, 496, 500-507.

[37] M. You, C. Chen, L. Xu, F. Mou, J. Guan, Acc. Chem. Res. 2018, 51, 3006-3014.

[38] M. H. Chang, D. Das, P. V. Varde, M. Pecht, Microelectron. Reliab. 2012, 52, 762-782.

[39] C. M. Huang, J. A. Romero, M. Osterman, D. Das, M. Pecht, Microelectron. Reliab. 2019, 99, 262-272.

[40] K. Bente, A. Codutti, F. Bachmann, D. Faivre, Small 2018, 14, 1704374.

[41] R. Blakemore, Science 1975, 190, 377-379.

[42] A. P. Chen, V. M. Berounsky, M. K. Chan, M. G. Blackford, C. Cady, B. M. Moskowitz, P. Kraal, E. A. Lima, R. E. Kopp, G. R. Lumpkin, B. P. Weiss, P. Hesse, N. G. F. Vella, Nat. Commun. 2014, 5, 4797.

[43] P. Dhar, Y. Cao, T. Kline, P. Pal, C. Swayne, T. M. Fischer, B. Miller, T. E. Mallouk, A. Sen, T. H. Johansen, J. Phys. Chem. C 2007, 111, 3607-3613.

[44] P. S. Schattling, M. A. Ramos-Docampo, V. Salgueiriño, B. Städler, ACS Nano, 2017, 11, 3973-3983.

[45] L. Baraban, D. Makarov, R. Streubel, I. Mönch, D. Grimm, S. Sanchez, O. G. Schmidt, ACS Nano 2012, 6, 3383-3389.

[46] G. Zhao, M. Pumera, Langmuir 2013, 29, 7411-7415.

[47] F. Peng, Y. Tu, Y. Men, J. C. van Hest, D. A. Wilson, Adv. Mater. 2017, 29,1604996.

[48] W. M. Ng, H. X. Che, C. Guo, C. Liu, S. C. Low, D. J. C. Chan, R. Mohamud, J. Lim, Langmuir 2018, 34, 7971-7980.

[49] Y. Lui, D. Ge, J. Cong, H. G. Piao, X. Huang, Y. Xu, G. Lu, L. Pan, M. Liu, Small 2018, 14, 1704546.

[50] T. Qui, T. C. Lee, A. G. Mark, K. I. Morozov, R. Münster, O. Mierka, S. Turek, A. M. Leshansky, P. Fischer, Nat. Commun. 2014, 5, 5119.

[51] S. Tottori, B. J. Nelson, Small 2018, 14, 1800722.